

# First- and second-order Poisson spots

William R. Kelly<sup>a)</sup>

*BBN Technologies, 10 Moulton Street, Cambridge, Massachusetts 02138*

Eric L. Shirley

*Optical Technology Division, NIST, 100 Bureau Drive, MS 8441, Gaithersburg, Maryland 20899-8441*

Alan L. Migdall and Sergey V. Polyakov

*Optical Technology Division, NIST, 100 Bureau Drive, MS 8441, Gaithersburg, Maryland 20899-8441 and Joint Quantum Institute, University of Maryland, College Park, Maryland 20742*

Kurt Hendrix

*Optical Technology Division, NIST, 100 Bureau Drive, MS 8441, Gaithersburg, Maryland 20899-8441*

(Received 8 July 2008; accepted 25 March 2009)

Although Thomas Young is generally given credit for being the first to provide evidence against Newton's corpuscular theory of light, it was Augustin Fresnel who first stated the modern theory of diffraction. We review the history surrounding Fresnel's 1818 paper and the role of the Poisson spot in the associated controversy. We next discuss the boundary-diffraction-wave approach to calculating diffraction effects and show how it can reduce the complexity of calculating diffraction patterns. We briefly discuss a generalization of this approach that reduces the dimensionality of integrals needed to calculate the complete diffraction pattern of any order diffraction effect. We repeat earlier demonstrations of the conventional Poisson spot and discuss an experimental setup for demonstrating an analogous phenomenon that we call a "second-order Poisson spot." Several features of the diffraction pattern can be explained simply by considering the path lengths of singly and doubly bent paths and distinguishing between first- and second-order diffraction effects related to such paths, respectively. © 2009 American Association of Physics Teachers.

[DOI: 10.1119/1.3119181]

## I. INTRODUCTION

Although Thomas Young was one of the first to present experimental evidence in support of the wave theory of light, his theory for explaining the observed phenomena did not quantitatively agree with many experimental results.<sup>1</sup> Fresnel, who based his work on a reinterpretation of Huygens' principle, developed a theory that better describes many wave phenomena and is still used today.<sup>2-4</sup>

In this paper we examine the implications of Fresnel's work, particularly the phenomenon of the Poisson spot. The term Poisson spot refers to a bright spot in the center of the geometric shadow of an opaque disk. If such a disk is illuminated by a point source, the center of the Poisson spot will theoretically be as intense as if there was no disk at all. The counterintuitive nature of the Poisson spot makes it a particularly effective demonstration of the wave theory of light.

We first discuss the controversy surrounding Fresnel's work, as well as the boundary-diffraction-wave (BDW) approach to calculating first- and second-order diffraction effects. We validate our results by obtaining agreement with a calculation using the Lommel function.<sup>3,5</sup> We then reproduce the first- and second-order Poisson spots based on an experimental setup involving an aperture located entirely within the shadow of an obscuring disk illuminated by a small source. We observe diffraction effects using a He-Ne laser with a roughly Gaussian intensity profile as an approximation for a point source,<sup>4,5</sup> and a commercially available camera for a detector.<sup>6</sup>

## II. BACKGROUND

### A. History

The Poisson spot was first discovered experimentally in 1723 by the mathematician-astronomer Miraldi.<sup>2</sup> At the time,

Miraldi's discovery went almost entirely unnoticed. Almost a hundred years later the Poisson spot was rediscovered. However, this time it was discovered theoretically.<sup>1</sup>

In 1818 Fresnel submitted a treatise, *Memoir on the Diffraction of Light*,<sup>1</sup> to the French Academy claiming that first-order diffraction effects could be calculated in accordance with Huygens' principle by integrating contributions from every possible singly bent path. Poisson, who was a member of the committee judging Fresnel's paper, realized that Fresnel's theory implied that there should be a bright spot in the center of the shadow of a circular disk. The occurrence of the spot can be calculated using Fresnel's theory, but it can more easily be seen by noticing that all secondary wave fronts originating along the edge of the disk will have the same phase. Thus, all contributions will constructively interfere, resulting in a bright spot as shown in Fig. 1.<sup>2</sup>

Poisson, who favored a particle treatment of light, believed that this counter intuitive prediction convincingly demonstrated the absurdity of the wave theory. Another member of the committee, Dominique Arago, conducted this experiment and observed the bright spot. This discovery effectively ended the wave-particle debate for the rest of the century, and the Poisson spot is named for a person who believed that it did not exist.<sup>2</sup>

Fresnel's paper refuted both Newton's corpuscular theory and Young's incomplete wave theory of light and produced a new theory based on Huygens' principle.<sup>1</sup> Fresnel's theory is still widely used today. The only difference between Fresnel's theory and contemporary diffraction theory is that Fresnel derived his laws by considering mechanical disturbances in the ether, whereas optics is now based on propagation equations which can be derived from Maxwell's equa-

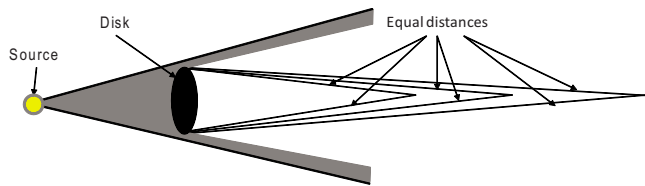


Fig. 1. For a point source on the symmetry axis of an opaque disk first-order light interferes constructively, resulting in a central bright spot (Poisson spot) along the optic axis.

tions. The two theories make identical predictions of diffraction effects. Polarization effects are beyond the scope of this paper.

Fresnel refuted Newton's corpuscular theory by noting that according to the latter, diffraction must be caused by attractive and repulsive forces that act on light particles in the immediate vicinity of an obstructing body. The dark regions must be explained by a force deflecting light particles away from those regions because particles cannot cancel each other. Fresnel noted that these disturbances should depend on the material makeup of the body and should cause the streams of light particles to move in straight lines. Neither of these conclusions are correct: the material from which the obstructing body is made does not significantly affect diffraction effects, and diffraction fringes trace out hyperbolic paths along the optic axis.<sup>1</sup>

In contrast, Young's theory treats light as a wave, but assumes that diffraction effects are caused solely by the deflection of light rays scattered by the surface of the obstructing body. Young concluded that within the geometrical shadow of a body, diffraction is caused by the interference of scattered rays with each other; outside of the geometrical shadow of a body diffraction is caused by the interference of scattered rays with primary rays as shown in Fig. 2.<sup>1</sup>

Young's theory successfully predicts the position of interference fringes in many experiments, most notably in the well known double-slit experiment. The results of this experiment agree with Young's theory when the slit widths are much smaller than the separation between slits. In this limit Young's theory gives correct results because each slit can be treated as a point source.

In general, Young's theory predicts the position of intensity minima and maxima in many diffraction experiments. Fresnel showed that Young's theory was incomplete by mak-

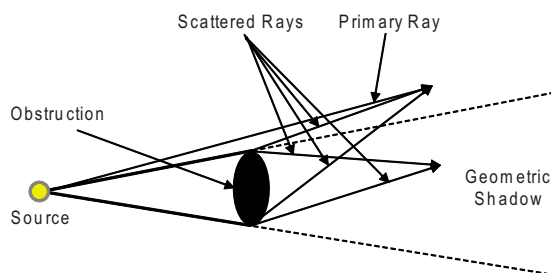


Fig. 2. Young's explanation of diffraction effects. Within the geometric shadow diffraction is caused by interference between secondary rays, or rays that are scattered by the obstruction. Outside of the geometrical shadow diffraction is caused by interference between scattered rays and primary rays. Although Young's theory successfully predicts the position of intensity minima and maxima in many cases, it fails to describe other features such as intensity and line width.

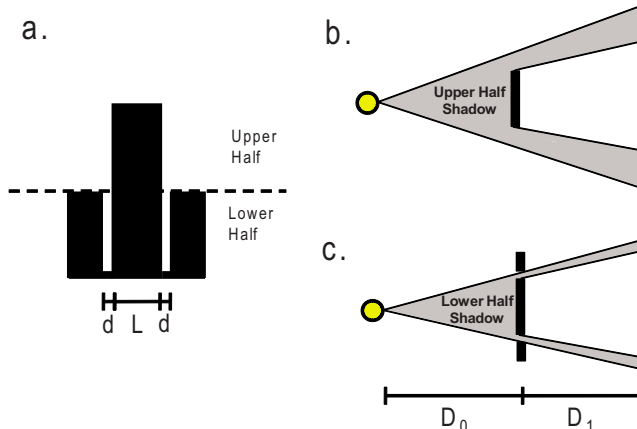


Fig. 3. (a) Fresnel showed the inadequacies of Young's theory by studying the diffraction pattern caused by a mask of this shape (front view). Fresnel compared the diffraction pattern (b) caused by illuminating the upper half of the mask, with (c) the pattern caused by illuminating the lower half. This experiment allowed him to observe the effect that light which does not pass near the obstruction (that is, light which is blocked by the lower half of the mask, but not by the upper half) has on the diffraction pattern.

ing quantitative observations of the intensity of diffraction effects. For example, Fresnel considered the diffraction effects caused by illuminating a copper mask of the shape shown in Fig. 3(a). Based on Young's theory we would expect the diffraction fringes produced by the lower half to be brighter and have wider fringes than those on the upper half. The lower fringes should be brighter because they would be caused by light scattered by four edges, whereas the upper diffraction effects would be caused by only two edges. Young's theory also predicts that the lower fringes would be wider because the narrow slits have nonzero width so that the light scattered by the inner and outer edges would not have exactly the same phase. All of these predictions are contradicted by experiment. This contradiction led Fresnel to conclude that Young's theory is fundamentally flawed.<sup>1</sup>

In reality, the fringes produced by the lower half are narrower than the fringes produced by the upper half. Also, when the detection plane is close to the mask, the fringes produced by the lower half are brighter than those produced by the upper half. As the detection plane is moved farther away from the mask, the intensity of the fringes produced by the lower half mask decreases until it is dimmer than the intensity of the fringes produced by the upper half. The condition for the intensities to be equal can be derived from the geometry of the source mask and detector as will be explained in the following. To explain this and other effects, Fresnel stated the following law, which he referred to as Huygens' principle:

"The vibrations at each point in the wave front may be considered as the sum of the elementary motions which at any one instant are sent to that point from all parts of this same wave in any of its previous positions, each of these parts acting independently the one of the other."<sup>1</sup>

Fresnel, like Huygens, imagined that a wave front was the leading edge of a wave of vibrations of the ether. Like Huygens, Fresnel believed that each point on the wave front caused its own secondary wave, which in turn led to the

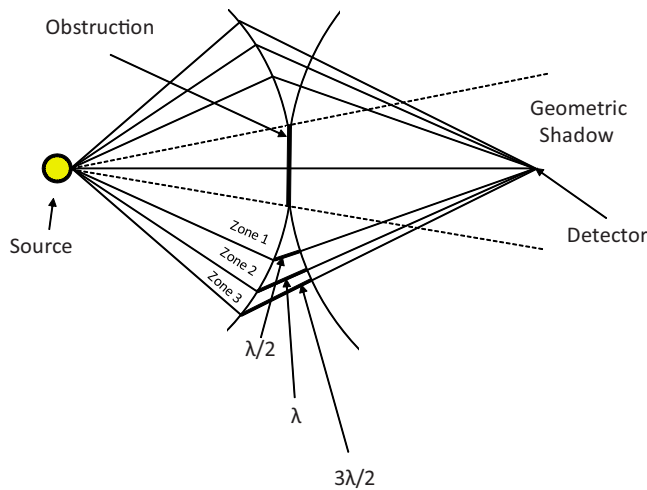


Fig. 4. A portion of the wave front is decomposed into three zones, each of which spans a phase difference of  $\pi$  radians; equivalently, the zones are divided by paths which differ in length by  $\lambda/2$ . Fresnel considered how waves from these zones would interfere to calculate the diffraction effect of the mask shown in Fig. 3. Fresnel used this decomposition to make predictions about the intensity, width, and position of the fringes of the resulting diffraction pattern.

propagation of the primary wave front. In free space the secondary waves caused by a spherical wave front would cancel except in the direction normal to the surface of the sphere. Thus, a spherical wave would continue to propagate as a sphere.<sup>1</sup>

Huygens asserted that the secondary waves would have a negligible effect except where they were exactly in phase. Fresnel considered contributions of secondary waves that are partially constructive or destructive, and found that he did not have to rely on the edge of an obstruction to reflect or scatter light. Instead he found that when an obstruction blocks part of a wave front, the precise cancellation of secondary waves that results in normal propagation is disturbed, and noticeable diffraction effects occur.<sup>1</sup>

Fresnel showed that his theory could account for the observed phenomena by breaking the wave front into zones of nearly uniform phase and calculating the interference of waves emitted from these zones (see Fig. 4). This approach is vastly simpler than integrating over the entire wave front, a calculation now known as the Kirchhoff integral, and for simple geometries gives a good approximation to the diffraction pattern. For a modern account of Fresnel zones see Ref. 2. It can be shown using this approach that the intensities of the fringes produced by the upper and lower halves of the diffraction mask should be approximately equal when half of the first Fresnel zone is blocked by the lower half mask. This equality approximately occurs when the path lengths from the inner and outer edge of the slits differ by  $\lambda/4$ , or when

$$d = \frac{\lambda}{2L} \frac{D_0 D_1}{D_0 + D_1}, \quad (1)$$

where  $d$  is the slit width,  $L$  is the spacing between the edges of the slits,  $D_0$  is the distance from the source to the plane of the mask,  $D_1$  is the distance from the plane of the mask to the detection plane,  $\lambda$  is the wavelength, and we have used the paraxial approximation and assumed that  $d \ll L$  (see Fig. 3).

For more details see Ref. 1, Fig. 22, and the accompanying explanation.

Although the Poisson spot is not mentioned in Fresnel's paper,<sup>1</sup> the existence of the spot provides another validation of Fresnel's theory. Young's theory predicts the existence of the Poisson spot, but also predicts that the intensity of the spot would change with the radius of the obstruction because a larger circumference would mean that more light is deflected toward the center, resulting in a brighter spot. In reality the intensity of the Poisson spot is constant if the radius of the disk is sufficiently small that the deflection angles are small.<sup>1</sup>

## B. Theory

The standard method of calculating diffraction effects is based on evaluating the Kirchhoff integral.<sup>7</sup> The Kirchhoff integral for a series of  $N$  parallel opaque disks or apertures is

$$U(\mathbf{r}_{N+1}) = \frac{U_0}{(i\lambda)^N} \int_{A_1} \cdots \int_{A_N} \frac{e^{ik\ell}}{d_0 \cdots d_N} dA_1 \cdots dA_N. \quad (2)$$

Here  $|U|^2$  is the intensity,  $U_0$  is related to the wave amplitude at the source,  $k=2\pi/\lambda$ , and  $d_j$  is the distance between the parallel planes  $j$  and  $j+1$ . Plane 0 contains the source, plane  $j$  contains aperture  $j$  for  $0 < j < N+1$ , and plane  $N+1$  contains the detector.  $A_j$  is the unobstructed area in plane  $j$ , and  $\ell$  is the total length of the line segments connecting the points  $\mathbf{r}_0, \mathbf{r}_1, \dots, \mathbf{r}_{N+1}$ , where  $\mathbf{r}_0$  is a position on the source,  $\mathbf{r}_{N+1}$  is a position on the detector, and  $\mathbf{r}_j$  is a point in the unobstructed region of plane  $j$ .

Equation (2) gives the amplitude of the wave at a particular point in the detector plane by integrating the phase contributions from all possible bent paths from the source to the point in question, allowing bends only in the plane of an obstruction. It is clear from Fig. 1 that the integral will predict the existence of the Poisson spot. Because path length, and therefore phase, is a function of the spatial position of the bend, the Kirchhoff integral necessitates integration over the entire unobstructed area. Thus for  $N$  apertures a  $2N$ -dimensional integral is necessary. This procedure can be streamlined using the arbitrary-order BDW approach given in Ref. 8. The essential features of this approach are a paraxial approximation of distances in exponents, and a separate calculation of each order of diffraction.

In an  $N=2$  source-aperture-aperture-detector setup, both first- and second-order effects must be considered. Light may be bent once at either of the two apertures, or it may be bent twice, once at each aperture. These effects are calculated using two separate integrals. If there is no geometrical blocking, that is, if the entire edge of the aperture is "visible" to the detector, the amplitudes from these integrals can be simply added. However, if there is geometrical blocking of the boundaries of any of the elements, only certain path lengths make contributions, which must be taken into account. As discussed in Ref. 8, the  $N$ th-order diffraction effect can be calculated using an  $N$ -fold integral, and this result must be combined with other order diffraction effects to give the complete result. In certain geometries effects at a given order might be completely blocked, making their calculation unnecessary. However, even if diffraction effects at all  $N$  orders have to be calculated using an  $N$ -fold integral for each, this calculation is a great computational improvement over the  $2N$ -fold Kirchhoff integral.

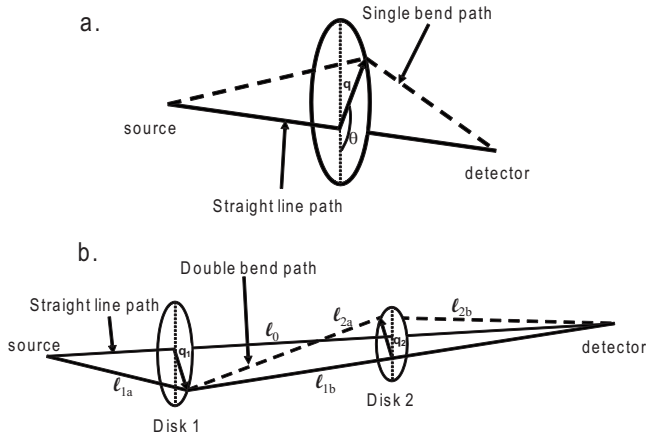


Fig. 5. (a) The single-bend path (dashed line) length is a function of the source position, detector position  $|\mathbf{q}|$ , and  $\theta$ . (b) In the second order case we must consider paths with two bends, one at each aperture (dashed line). A bend is first introduced at disk 1 and then at disk 2. Calculation of second-order effects must also include a contribution from the integral in which a bend is at disk 2 first, and then at disk 1. The stationary paths (see text) occur where the first derivatives of the path length with respect to all angles of integration are zero. (a) In the first-order case this condition is met when  $|\mathbf{q}|$  is at a maximum or minimum. (b) If both disks are displaced along the same axis in the second-order case, the minimum and maximum path lengths occur when  $\mathbf{q}_1$  and  $\mathbf{q}_2$  lie on the diameters indicated by dotted lines.

To understand how the reduction from a  $2N$ -fold integral to an  $N$ -fold integral takes place, it is instructive to examine the first-order case in detail. For a single obstruction the diffraction effect is a result of all singly bent paths with the bend in the plane of the obstruction. In the paraxial approximation the path length is a function of the distance from the intersection of the unbent path and the plane of the obstruction to the point at which the bend occurs if the position of the source and detector are given. This distance is represented by the vector  $\mathbf{q}$  in Fig. 5. The path length is of the form

$$\ell = \alpha + c|\mathbf{q}|^2, \quad (3)$$

where

$$c = \frac{1}{2d_0} + \frac{1}{2d_1}, \quad (4)$$

and  $\alpha$  is the straight line path length from the source to the detector. Equation (3) may be substituted into Eq. (2) to calculate the diffraction effects of a single disk. This integral is best done in cylindrical coordinates by replacing  $dA_1$  with  $r_1 dr_1 d\theta_1$ , where  $r_1 = |\mathbf{q}|$ . This substitution gives

$$U(\mathbf{r}_2) = \frac{U_0 e^{ik\alpha}}{i\lambda d_0 d_1} \int_0^{2\pi} \int_{R(\theta)}^{\infty} e^{ikc r_1^2} r_1 dr_1 d\theta_1, \quad (5)$$

where we have used  $R(\theta)$  as the lower limit of the radial integral to indicate that if the source or the detector is off-axis, then the radial limits of integration depend on  $\theta$ . Both  $\alpha$  and  $R(\theta)$  depend on  $\mathbf{r}_2$ . Because the integrand is Gaussian in form, the radial integral can be done analytically, leaving a single angular integral:

$$U(\mathbf{r}_2) = -\frac{U_0 e^{ik\alpha}}{4\pi d_0 d_1 c} \int_0^{2\pi} e^{ikc(R(\theta_1))^2} d\theta_1. \quad (6)$$

Thus, an area integral has been reduced to a single angular integral. In the off-axis case, this integral must be computed numerically; if the disk and detector are on axis, the angular integration is equivalent to multiplying by  $2\pi$ . When this result is multiplied by its complex conjugate to obtain the intensity, we obtain

$$|U(z)|^2 = \frac{|U_0|^2}{z^2}, \quad (7)$$

where

$$z = d_0 + d_1. \quad (8)$$

This calculation shows that according to Fresnel's theory, the on-axis intensity is unaffected by the presence of the disk, or in other words, the center of the Poisson spot is as bright as if there were no disk at all.

Reference 8 generalizes this approach to arbitrarily high-order diffraction effects. The complete generalization is beyond the scope of this paper, but we will state the form of the general result and give the integral for calculating second-order effects.

The key to our success in the first-order case was our choice of origin for the polar coordinates. By choosing the origin as a point along  $\alpha$  we ensured that  $\ell$  would depend only on  $|\mathbf{q}|^2$  and not on  $|\mathbf{q}|$ . Consequently, the Kirchhoff integral was Gaussian in form and the integration reduced to division by a factor proportional to  $ikc$ . For higher-order diffraction effects this approach is not sufficient because multiple bends must be introduced into the path, complicating the choice of origin. Figure 5(b) illustrates one of two choices in which bends can be introduced into a path from source to detector with two obstructions. The first bend changes the path from  $\ell_0$  to  $\ell_{1a} + \ell_{1b}$ ; the second bend further changes the path to  $\ell_{1a} + \ell_{2a} + \ell_{2b}$ . It is shown in Ref. 8 that when the path length is written in this form and the paraxial limit applies, then the radial integrals can be calculated analytically and the remaining integral has the form:

$$\Delta U(\mathbf{r}_{N+1}) = \frac{U_0}{(i\lambda)^N} \int_0^{2\pi} \int_{R_1(\theta_1)}^{\infty} \cdots \int_0^{2\pi} \int_{R_N(\theta_N)}^{\infty} \frac{e^{ik\ell}}{d_0 \cdots d_N} \times r_1 dr_1 d\theta_1 \cdots r_N dr_N d\theta_N \quad (9a)$$

$$= \frac{(-1)^N U_0}{(4\pi)^N d_0 \cdots d_N} \int_0^{2\pi} \cdots \int_0^{2\pi} G e^{ik\ell(\{R_j(\theta_j)\})} d\theta_1 \cdots d\theta_N, \quad (9b)$$

where  $G$  depends on the geometry of the setup and on the angular coordinates, and  $\ell(\{R_j(\theta_j)\})$  denotes a path with bends introduced sequentially at each of the  $N$  disks or apertures. Equation (9b) is the same form as Eq. (15) in Ref. 8 in which a general expression is given for  $G$ . This integral gives one contribution to the  $N$ th-order diffraction effects. Other contributions are formed by changing the order in which the bends are introduced in the path. Changing the ordering does not affect  $\ell$ , but affects  $G$  and the differentials  $\{d\theta_j\}$ . Lower-order effects must be calculated separately and added to this integral to give the complete diffraction pattern.

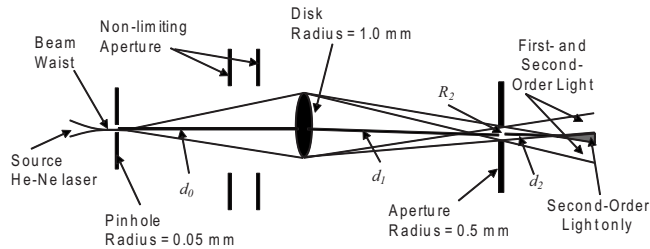


Fig. 6. A schematic diagram of our experimental setup. The disk, aperture, and detector (not shown) were placed on three-dimensional translation stages to give complete control over the geometry of the setup.

Note that  $\ell$  in Ref. 8 is used to denote the reduced path length, which in our notation is  $\ell - \alpha$ .

In the second-order case the contribution corresponding to Fig. 5 can be written as

$$\Delta U(\mathbf{r}_3) = \frac{U_0 e^{ik\ell_0}}{(4\pi)^2 d_0 d_1 d_2} \int_0^{2\pi} \int_0^{2\pi} \frac{|\mathbf{q}_1|^2 |\mathbf{q}_2|^2 e^{ik(\ell_{1a} + \ell_{2a} + \ell_{2b} - \ell_0)} d\theta_1 d\theta_2}{(\ell_{1a} + \ell_{2a} + \ell_{2b} - \ell_0)(\ell_{2a} + \ell_{2b} - \ell_{1b})}, \quad (10)$$

where  $\mathbf{q}_1$  and  $\ell_{1a,b}$  depend on  $\theta_1$  and  $\mathbf{q}_2$  and  $\ell_{2a,b}$  depends on  $\theta_2$ . In contrast to Eq. (6) which gives the first-order BDW, Eq. (10) illustrates how the second-order BDW is calculated. These integrals were computed numerically and added where appropriate (when the wave were not geometrically blocked) to obtain the theoretical predictions shown in Sec. IV.<sup>9</sup>

When one or more of the obstructions does not lie along the  $z$ -axis, the value of the angular integral can be approximated using the method of stationary phase<sup>10</sup> if  $\lambda$  is small compared to the characteristic length given by the square of the radius of the smallest disk or aperture divided by the largest distance between elements. In this case a small change of the path length results in a large change in phase because  $k=2\pi/\lambda$ . Thus, the integrand consists mostly of rapid oscillations which average to zero, with the exception of stationary points where the gradient is zero. In our experiments  $\lambda$  was approximately half of this characteristic length, and the method of stationary phase still gives a good approximation for the intensity.

In the first-order case the stationary points occur at the minimum and maximum values of the radial component. In the second-order case, in which only one of the obstructions is off-axis, the stationary points occur when  $\mathbf{q}_1$  and  $\mathbf{q}_2$  lie along the axis of displacement (see Fig. 5). In the first-order case the integral can be approximated by replacing  $\ell$  in the integrand with the first three terms of its Taylor series approximation. In the second-order case the first derivatives are still zero and the volume under the stationary points can be determined analytically by an analogous process. This method cannot be used if both apertures or masks are on-axis. In this case there are an infinite number of stationary points which occur whenever  $\theta_1 = \theta_2$  or  $\theta_1 = \theta_2 \pm \pi$ . For this approximation to be efficient at least one of the masks must be off-axis. For setups in which both masks are off-axis, the locations of the stationary points might not be obvious. In this case stationary points must be found using more sophisticated analytic techniques or a numerical search.

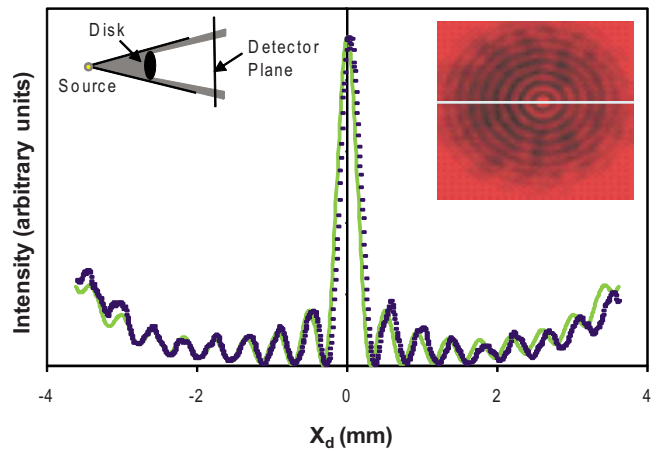


Fig. 7. (Color online) Measured (points) and calculated (line) first-order diffraction from a disk. Inserts: (Left) A schematic of the experimental setup. (Right) An image of the Poisson spot and surrounding rings, with a white line indicating the location of the intensity cross section here and in following figures. The close agreement between theory and measurement is evidence that we successfully approximated a point source. In this plot and all following intensity plots the calculated intensity was scaled to fit the experimental data. This vertical scaling was done by matching intensities of the minima adjacent to the central peak of the two curves. A horizontal offset was necessary to make the curves match, but no vertical offset or horizontal scaling were used. In the case of asymmetry the maximum (right or left) which gave a better overall fit was chosen.

### III. EXPERIMENTAL DEMONSTRATION

To ensure that second-order effects can be observed apart from first-order effects, our experimental setup consists of an opaque disk followed by an aperture placed entirely within the geometric shadow of the disk. Thus, a certain distance beyond the aperture there is a circular region which can be reached only by second-order light. That is, for light to reach that region, its path must bend twice, once at the disk and once at the aperture (see Fig. 6).

A number of disk and aperture sizes were created by evaporating metal onto glass plates. The metal consisted of a 20 nm layer of titanium followed by 130 nm layer of aluminum. The type of metal used is unimportant as long as the masks are completely opaque and the mask thickness times the angle by which the diffracted rays are bent is small compared to the wavelength. First-order effects can be observed using a U.S. penny as a diffraction mask.<sup>5</sup> Our disks ranged from 0.2 to 1.5 mm in radius and the apertures ranged from 0.05 to 0.75 mm in radius. Our light source was a He-Ne laser with an output wavelength of 633 nm and an output power of  $\approx 5$  mW. The intensity profile of the source was roughly Gaussian, in contrast to the theory which assumes a nearly flat intensity profile. To approximate uniform intensity, the beam was focused to a waist with a radius of  $\approx 1$  mm and limited by a pinhole with a 0.05 mm radius. The disk was carefully centered in the beam to ensure that the intensity around the perimeter of the disk was uniform. Therefore, as long as the aperture was placed entirely in the shadow of the disk, the actual source behaved as a point source. The reason this approximation is valid is because the edge of the disk was uniformly illuminated, as it would be by a point source, and the effect of light far away from the edge of the disk is negligible. The first-order diffraction effects were similar to those of a point source, as was confirmed by our measurements (see Fig. 7).

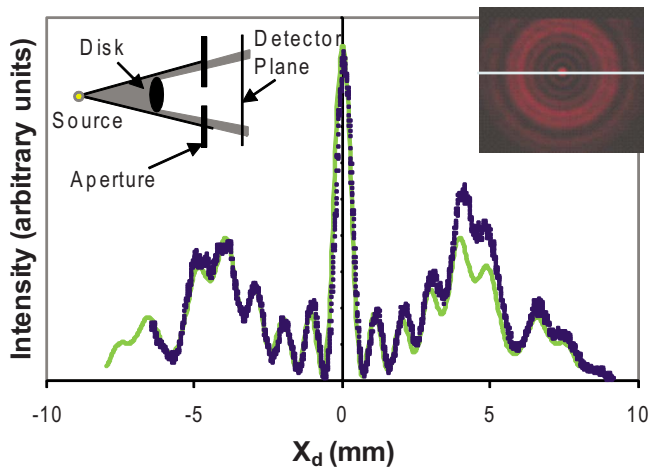


Fig. 8. (Color online) Measured (points) and calculated (line) intensity. Inserts: (Left) A schematic of the experimental setup. (Right) An image of the second-order Poisson spot and surrounding rings.

The waist of the beam, truncated by a pinhole, was treated as a point source and the phase was assumed to be uniform across the pinhole. In actuality, our source was not a point but rather a circle with radius 0.05 mm. Calculations that treat the source as a collection of in-phase point sources covering the area of the pinhole changed the fringe heights in the diffraction intensity distribution by at most on the order of 1%. Two nonlimiting apertures, that is, apertures that did not intersect the beam, were used to block Airy rings caused by the pinhole and other stray light from reaching the other disks on the glass plate. By placing the edge of the nonlimiting apertures in the dark regions of the Airy rings we ensured that diffraction effects from these apertures were negligible. These nonlimiting apertures had radii of 25 to 50 mm, and because the intensity of the beam falls off exponentially with radial distance, diffraction effects from these apertures were negligible. The apertures were placed approximately 5 and 10 cm upstream from the disks.

To best approximate a point source it is important that the intensity around the edge of the disk be uniform. This uniformity was achieved by expanding the first-order pattern using mirrors to reflect it several times and adjusting the position of the disk so that the Poisson spot appeared at the center of the beam.

The aperture was centered in the shadow of the disk by adjusting the aperture position until the second-order spot was centered within the brighter annular region of the first-order light. Once the aperture was centered we displaced it along the  $x$ -,  $y$ -, and  $z$ -axes using translation stages, and the measured displacements were used in our calculations.

Our detector was a commercial single lens reflex digital camera with the objective lens removed and a pixel pitch of  $7.8 \times 7.8 \mu\text{m}^2$ . We were able to export the image data from the camera in a raw format that retained the linear response for comparison with our calculations using a program called NEFRead.<sup>11</sup>

#### IV. RESULTS

We first present first-order diffraction effects in the geometric shadow of the disk with no aperture present (see Fig. 7). The observed effects show that we can reproduce the diffraction pattern of a point source using a Gaussian beam.

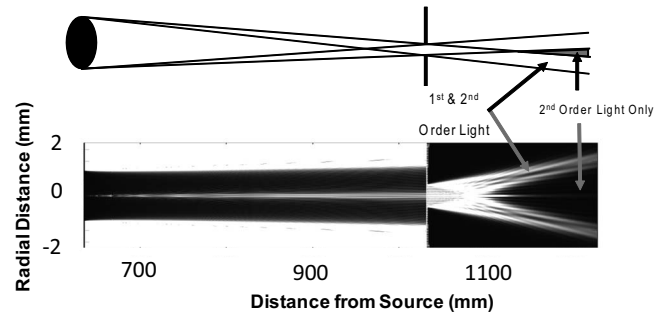


Fig. 9. Interference of first- and second-order light shown schematically (top) and computer-simulated (bottom). The bottom figure shows the  $x$ - $z$  cross section of the Poisson spot on the left side. The Poisson spot is then incident on an aperture resulting in the second-order effect to the right. The brightness scale of the right-hand section was rescaled to make the second-order effects visible.

The agreement between theory and experiment was very close in the geometric shadow. Outside the shadow the intensity falls off exponentially, whereas a point source would approach a finite intensity. This fall off is immaterial so long as the detector is placed entirely within the shadow of the disk.

We next inserted an aperture in the geometric shadow of the disk (see Fig. 8). The second-order diffraction pattern consists of a region of exclusively second-order light in which there is a central bright spot, much like the first-order

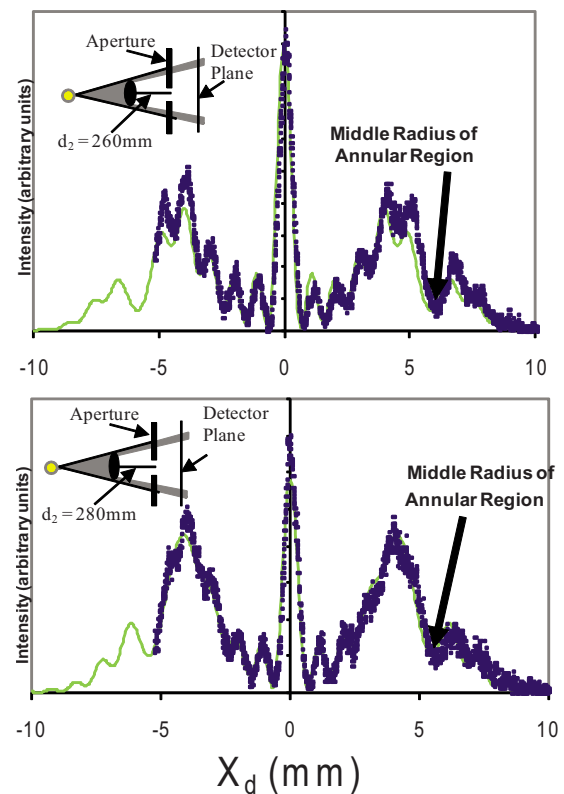


Fig. 10. When  $R_2=0.5$  mm first- and second-order light are approximately  $\pi$  radians out of phase. Measured (points) and calculated (line) data are shown for two values of  $d_2$ . The same vertical scaling factor was used for the top and bottom plots. (Inserts) Schematics of the experimental setup with  $2-2 \cos(u/2)=0.355$  or  $0.580$  for  $d_2=260$  mm or  $d_2=280$  mm, respectively.

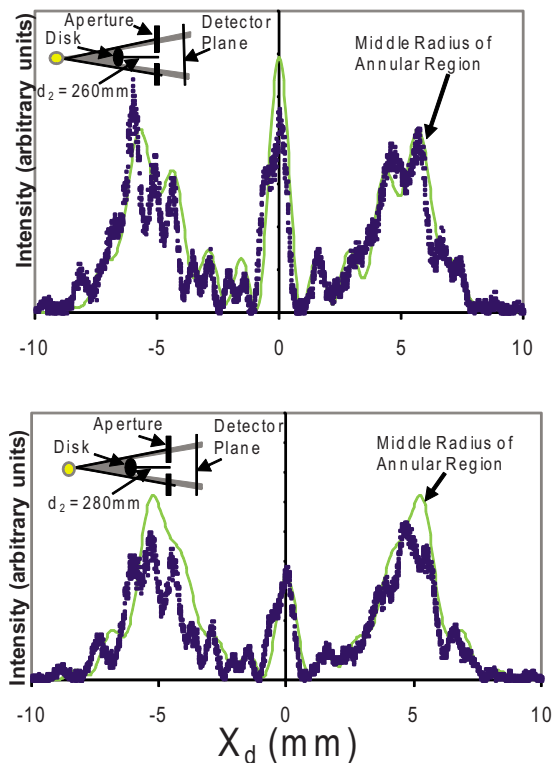


Fig. 11. When  $R_2=0.35$  mm first- and second-order light are approximately in phase. Measured (points) and calculated (line) data are shown for two values of  $d_2$ . The same vertical scaling factor was used for the top and bottom plots. (Inserts) Schematics of the experimental setup with  $2-2\cos(u/2)=3.872$  or  $3.730$  for  $d_2=260$  mm or  $d_2=280$  mm, respectively. The origin of the additional observed fringing in the figure is not clear.

pattern. Surrounding the second-order region is an annulus in which there is interference between first- and second-order light. The on-axis results show very close agreement between experiment and theory, except for some asymmetry which might arise because of a very slight misalignment.

The presence and behavior of the annular region can be understood by considering the first- and second-order effects separately. Figure 9 shows an  $x$ - $z$  cross-section of an on-axis setup with the  $y$ -axis being the optical axis. Downstream from the aperture there is a cone in which the entire edge of the disk would be visible. In this region first-order light is entirely unblocked and the effects of the second-order light are negligible. Downstream of this region is another cone in which none of the edge of the disk is visible. In this region all first-order light is blocked and therefore all effects are second-order. Lastly, there is a region in which only part of edge of the disk is visible. In this region the amplitudes of first- and second-order light are comparable and interfere noticeably.

The inner and outer perimeters of the annular region can be determined directly from the geometry of the experimental setup. Between the perimeters the intensity in the annular region can exhibit a radial dependence because first- and second-order light can interfere constructively or destructively. To understand how this interference changes with the geometry, we approximate the intensity on the circle halfway between these perimeters. Along this circle the character of the interference can be estimated by treating each point on the edge of the disk as a point source. The plane of the aperture is not normal to the direction of propagation; given

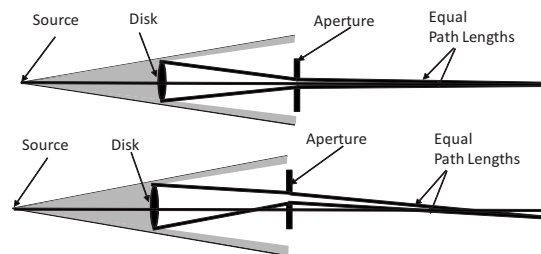


Fig. 12. The second-order Poisson spot, like the first-order Poisson spot, is caused by constructive interference because of equal path lengths. Opposite to the case of the first-order Poisson spot, the geometry of the setup dictates that second-order Poisson spot is moved down when the aperture is moved up, an effect that we observed.

that the radius of the disk is 1.1 mm and that the distance between the disk and the aperture is about 275 mm, the inclination of the aperture is only  $\approx 0.004$  rad. Thus, the interference can be characterized using an approximation for a source-aperture-detector setup, for which it has been shown<sup>12</sup> that the on-axis intensity is proportional to  $2-2\cos(u/2)$ , with  $u=k(R_2)^2(1/d_1+1/d_2)$ . Here  $R_2$  is the radius of the aperture,  $d_1$  is the distance from the edge of the disk to the center of the aperture, and  $d_2$  is the distance between the center of the aperture and the detector. Because of the relative lengths of the radii and the separation between elements in our experiment, it is an acceptable approximation to use the lengths along the optic axis for  $d_1$  and  $d_2$  (see Fig. 6).

We see that by altering  $d_1$ ,  $d_2$ , or  $R_2$ , while keeping the wavelength constant, the intensity in the middle radius of the annulus can be maximized or minimized. When  $2-2\cos(u/2)=0$ , the interference is purely destructive, and when  $2-2\cos(u/2)=4$ , the interference is purely constructive (see Figs. 10 and 11).

Our calculations show that the intensity of the central spot oscillates as the distance between the disk and the aperture is changed. The reason for this oscillation is that as the aperture is moved closer or farther from the disk, its edge will alternately be illuminated by light and dark regions of the first-order diffraction pattern in the plane of the aperture. This change in intensity of the central spot can be seen in Fig. 11, but is somewhat obscured by asymmetry and additional fringing. It is likely that this deviation from the calculated

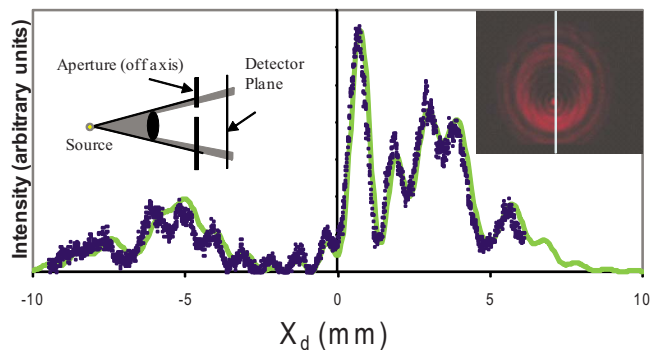


Fig. 13. (Color online) Measured (points) and calculated (line) intensity values for an off-axis second-order Poisson spot. Inserts: (Left) A schematic of the experimental setup. (Right) An image of the second-order off-axis Poisson spot. Interference can clearly be seen between the combined first- and second-order effects (the bright annular region) and exclusively second-order effects (the bright spot and concentric rings).

intensity was due to a slight misalignment in the aperture. Regrettably, we did not repeat this measurement, Fig. 11 shows general agreement between our results and the qualitative features we have described.

The observed off-axis behavior of the diffraction pattern further demonstrates the validity of the BDW formulation. When the aperture is moved off-axis to the right, the annulus moves to the right, but the Poisson spot moves to the left because the Poisson spot occurs where all second-order light is in phase. When the aperture is moved to the right, there will be a spot on the left where all of the path lengths are equal, because the second-order rays are primarily spread by the aperture, whereas first-order rays are concentrated by the disk (see Fig. 12). The movement of the spot and annular region supports the idea that the central spot is a second-order effect, whereas the annular region is a combination of first- and second-order effects. Figure 13 shows an image of an off-axis pattern in which interference between the second-order ring pattern and the ring pattern in the annular region is clearly visible. This effect further supports the claim that these two patterns have separate causes rooted in the geometry of the setup.

## V. CONCLUSION

The historical importance of the first-order Poisson spot to the wave theory of light, and a method of calculating the BDW integrals for higher-order diffraction effects using an  $N$ -fold integral was described. The advantages of this approach over the standard Kirchhoff integral makes the BDW approach a valuable tool for laboratory setups in which multiple apertures are used in series, such as in blackbody calibration or in spatial filtering. A knowledge of the causes of these effects can help an experimenter avoid or minimize undesired diffraction. The validity of the BDW approach for calculating higher-order diffraction patterns was demonstrated by the overall agreement between the experimental data and calculations, and our demonstration can be interpreted using a second-order BDW formulation. We suc-

ceeded in spatially isolating first- and second-order light and demonstrating second-order effects by using a disk and aperture in its shadow region.

## ACKNOWLEDGMENTS

The authors thank Richard Mirin of NIST Boulder for providing the masks and apertures for the experiment and Emily Tordo of the Boston Museum of Science for locating an English translation of Fresnel's 1818 paper. The authors also thank the anonymous reviewers of this paper for a great deal of thoughtful feedback that led to substantial improvements. One of the authors (W.R.K.) would like to acknowledge the support of a St. John's College's Hodson Trust Internship Program for making this work possible.

<sup>a)</sup>Electronic mail: wkelly@bbn.com

<sup>1</sup>An English translation of Huygens' *Treatise on Light* and Fresnel's *Memoir on the Diffraction of Light* can be found in H. Crew, *The Wave Theory of Light* (American Book Company, New York, 1900), pp. 79–144.

<sup>2</sup>E. Hecht, *Optics*, 4th ed. (Addison-Wesley, San Francisco, 2001).

<sup>3</sup>M. A. Heald, "Computation of Fresnel diffraction," *Am. J. Phys.* **54**(11), 980–983 (1986).

<sup>4</sup>J. E. Harvey and J. L. Forgham, "The spot of Arago: New relevance for an old phenomenon," *Am. J. Phys.* **52**(3), 243–247 (1984).

<sup>5</sup>P. M. Rinard, "Large-scale diffraction patterns from circular objects," *Am. J. Phys.* **44**(1), 70–76 (1976).

<sup>6</sup>G. R. Wein, "A video technique for the quantitative analysis of the Poisson spot and other diffraction patterns," *Am. J. Phys.* **67**(3), 236–240 (1999).

<sup>7</sup>M. Born and E. Wolf, *Principles of Optics*, 6th ed. (Pergamon, Oxford, 1980) pp. 375–386.

<sup>8</sup>E. L. Shirley, "Higher-order boundary-diffraction-wave formulation," *J. Mod. Opt.* **54**(4), 515–527 (2007).

<sup>9</sup>See EPAPS Document No. E-AJPIAS-77-011906 for simulation software. For more information on EPAPS, see [www.aip.org/pubservs/epaps.html](http://www.aip.org/pubservs/epaps.html).

<sup>10</sup>See Ref. 7, pp. 752–754.

<sup>11</sup>NEFRead is open source and available at [scien.stanford.edu/class/psych221/projects/07/camera\\_characterization/code.html](http://scien.stanford.edu/class/psych221/projects/07/camera_characterization/code.html).

<sup>12</sup>L. P. Boivin, "Diffraction correction in radiometry: comparison of two different methods of calculation," *Appl. Opt.* **14**, 2002–2009 (1975).